Exploring direct band gap engineering in chloro-elpasolite Cs_2(Ag,Au) $InCl_6$: A comprehensive study of structural, elastic, optoelectronic, and thermoelectric properties

N. Mechehoud[a], M. Hamdi Cherif[a], A. Zitouni[a], Z. Aziz[a,*], B. Bouadjemi[a], M. Houari[a,b], S. Haid[a,c], M. Matougui[a], T. Lantri[a,b], and S. Bentata[a]

[a]*Laboratory of Technology and Solid's Properties, Faculty of Sciences and Technology, Abdelhamid Ibn Badis University, BP 227, Mostaganem 27000, Algeria.*
[b]*Laboratory of Physics Thin Layer & Advanced Technologies, University of Relizane, Relizane, 48000, Algeria.*
[c]*Faculty of Sciences and Technology, Ahmed Ben Yahia El-Wancharissi University of Tissemsilt, Tissemsilt, 38000, Algeria.*
[*]*e-mail: zoubir.aziz@univ-mosta.dz*

Received 1 January 2022; accepted 9 February 2022

This study examined the stability, structural, electrical, optical, and thermoelectric characteristics of the halide double perovskites (HDPs) Cs_2BInCl_6, where B stands for Ag and Au. The Wien2k code package was used to conduct the investigation using the FP-LAPW technique, which is a subset of density functional theory (DFT). These compounds exhibit a crystalline structure within an elpasolite-type lattice, with a cell parameter of $a = 10.6005$ Å for $Cs_2AgInCl_6$ and $a = 10.6356$ Å for $Cs_2AuInCl_6$. The most stable configuration is characterized by a cubic structure with $Fm\bar{3}m$ (No. 225) symmetry in a non-magnetic (NM) state, as established by analyzing the optimal structural parameters for both materials.

Furthermore, an evaluation of the mechanical and elastic properties reveals the anisotropic and ductile nature of these substances. The negative results obtained from the formation energy calculations support the successful synthesis of $Cs_2AgInCl_6$ and the possibility of producing $Cs_2AuInCl_6$. The examination of the electronic features illustrates a semiconductor behavior characterized by a direct band gap at the Γ–Γ direction, with values of 3.245 eV for $Cs_2AgInCl_6$ and 2.052 eV for $Cs_2AuInCl_6$, closely mirroring experimental observations.

Furthermore, optical computations demonstrate an absorption coefficient within the visible spectrum that is almost zero and exceeds 1.6×10^4 cm^{-1} in the extreme ultraviolet (EUV) range. Moreover, the high reflectivity of the materials, reaching a peak of 55% for $Cs_2AgInCl_6$ and 40% for $Cs_2AuInCl_6$ at 17.5 eV (70.85 nm) in the EUV region, indicates a promising potential for utilization in optoelectronics, particularly in the UV and EUV sectors.

Additionally, the assessment of thermoelectric performance revealed that both perovskites exhibit elevated electrical conductivity, low thermal conductivity, an increased Seebeck coefficient, and a higher figure of merit, positioning them as favorable candidates for thermoelectric applications.

Keywords: Halide double perovskites; fp-lapw method; elastic behavior; optoelectronic properties; thermoelectric applications.

DOI: https://doi.org/10.31349/RevMexFis.72.010501

1. Introduction

Perovskites have garnered significant attention in recent years due to their unique optical and electronic properties [1], particularly halide double perovskites (HDPs) along with their potential applications in diverse fields [2]. These materials, officially called elpasolites [3], characterized by the structure $A_2M^IM^{III}X_6$ (where A is a large monovalent cation in the perovskite A site, M^I is a monovalent metal, M^{III} is a trivalent metal, and X is a halide (F, Cl, Br, I) [4]), exhibit promise in a range of applications beyond outdoor photovoltaics. These applications include temperature and humidity sensors, light-emitting diodes (LEDs), memory devices, indoor photovoltaics, X-ray detectors, and photocatalysts [5].

Lead-free halide perovskites represent a pivotal advancement in the pursuit of environmentally sustainable alternatives to conventional lead-based perovskites [6]. Notably, quaternary alloys such as $Al_xIn_{1-x}P_ySb_{1-y}$ and $Al_xGa_{1-x}P_ySb_{1-y}$ [7] exemplify this progress, offering remarkable versatility in tailoring both physical and electronic properties. Such tunability is crucial for improving the efficiency and stability of photovoltaic devices, particularly in multi-junction architectures and applications requiring broad solar spectrum absorption.

Our compound under study, $Cs_2AgInCl_6$, was successfully synthesized through different methods on multiple occasions. Initially, in 2017, G. Volonakis employed the precipitation technique [8], followed by the hydrothermal approach [9, 10], and the solid-state method [11, 12]. While the other compound $Cs_2AuInCl_6$ was studied for the first time. A number of similar HDP structures were successfully synthesized including $Cs_2CuBiCl_6$ [13], $Cs_2AgSbCl_6$ [14], and $Cs_2AgBi(Cl,Br)_6$ [15, 16].

Additionally, several theoretical investigations, like $Cs_2AgGa(Cl,Br)_6$ [17, 18], A_2AuScX_6 (A = Cs, Rb; X = Cl, Br, I) [19], $Cs_2AgAsCl_6$ [20], Rb_2AgGaX_6 [21], and $Cs_2AuBiBr_6$ [22], have been conducted. The Chloro-elpasolite Cs_2BInCl_6 (B = Ag, Au), with their direct band gaps, improve their potential for use in a variety of optical field applications [23, 24]. Understanding the optical characteristics of materials is essential for their use in various applications [25]. This property is crucial in the development

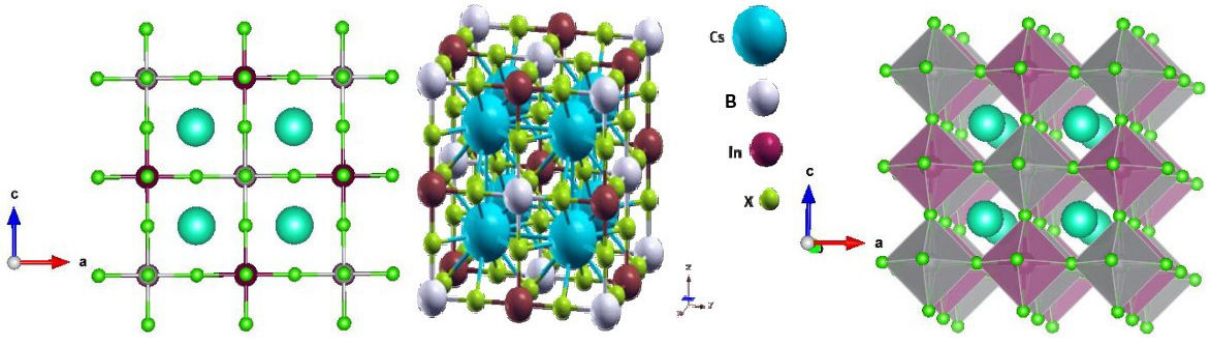

FIGURE 1. Crystalline cell of double perovskite Cs_2BInCl_6(B=Ag, Au).

of efficient solar cells, where maximizing light absorption is paramount for improved power conversion efficiency [26]. Moreover, the high reflectivity of the materials highlights their potential for use in optical applications [23]. The ability to efficiently reflect a significant amount of radiation provides a benefit for the progression of diverse optical uses, such as mirrors and lenses. These optical elements play a crucial role in sophisticated lithography methods utilized in the production of semiconductors [21].

The objective of this study is to investigate the structural, electronic, elastic, optical, and thermoelectric properties of the chloro-elpasolite Cs_2(Ag, Au)$InCl_6$, with a focus on the thermoelectric properties and the direct band gap and its importance in optical applications. Gaining a comprehensive understanding of this material's features will enable them to reach their full potential and support the development of optical and thermoelectric technologies.

2. Computational methods

All calculations in this work were conducted using the full potential linear augmented plane wave (FP-LAPW) method, which is based on density functional theory (DFT) [27]. The calculations were performed using the WIEN2K package [28]. The structural properties were calculated using the Generalized Gradient Approximation developed by Perdew–Becke–Ernzerhof (GGA-PBE) [29], in comparison with the well-known Tran–Blaha modified Becke–Johnson (TB-mBJ) exchange potential, leading to results that exhibit a closer correlation to experimental values. The optical and thermoelectric properties were analyzed using the modified Becke–Johnson (mBJ) exchange potential, providing accurate predicted insights.

Initialization was performed using the following parameters: bond length factor of 3, energy required for valence and core state separation of -6.0 Ry, $R_{\rm MT}K_{\rm max} = 7$ (where $R_{\rm MT}$ represents the average radius of the muffin-tin sphere and $K_{\rm max}$ indicates the maximum magnitude of the wave vector), number of employed k-points of 3000 ($17 \times 17 \times 17$), and the charge density's Fourier expansion limited to $G_{\rm max} = 12$ a.u.$^{-1}$. Moreover, we selected the muffin-tin radii values as follows in order to prevent overlap: 2.14 for Cl and 2.50 for Cs, Ag, Au, and In atoms.

Our compounds Cs_2BInCl_6, under study, crystallize in the cubic structure with space group $Fm\bar{3}m$ (No. 225) [30], as illustrated in Fig. 1. The unit cell contains two octahedra: one $InCl_6$ and the other BCl_6. These two octahedra alternate along the different crystallographic planes [100], [010], and [001] [8, 31]. The constituent atoms are positioned as follows: two Cs (Cesium) atoms are located at $8c$ $(\frac{1}{4}, \frac{1}{4}, \frac{1}{4})$ and $(\frac{3}{4}, \frac{3}{4}, \frac{3}{4})$, One Ag (Silver) atom or Au (Gold) is positioned at $4a$ $(0, 0, 0)$, one In (Indium) atom is at $4b$ $(\frac{1}{2}, \frac{1}{2}, \frac{1}{2})$, and six Cl (Chlorine) atoms occupy the positions $24e$ $(x, 0, 0)$ [32, 33].

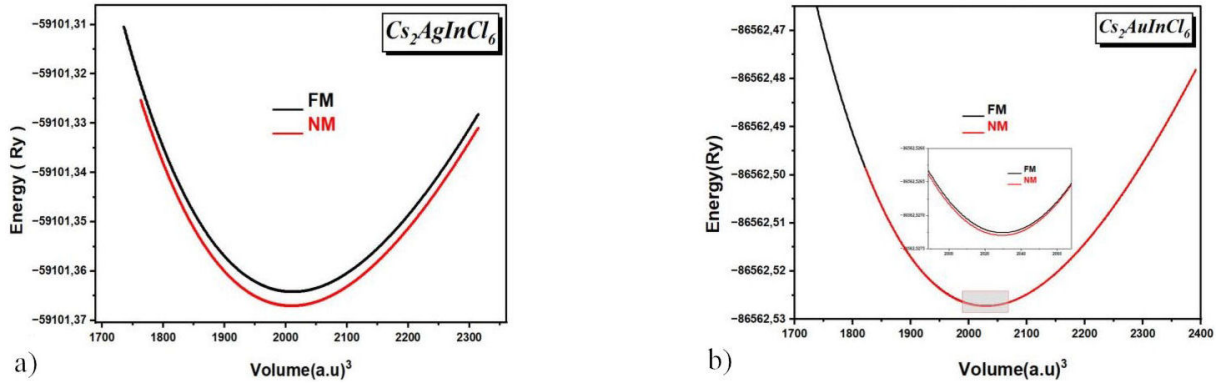

FIGURE 2. Energy versus volume Curve for Cs_2BInCl_6: a) For $Cs_2AgInCl_6$, b) For $Cs_2AuInCl_6$.

TABLE I. Calculated and experimental results for lattice constant a_0 (Å), bulk modulus B_0 (GPa), pressure derivative of bulk modulus B', tolerance factor t_G, octahedral factor μ, and formation energy E_{Form} (eV/atom) of $Cs_2AgInCl_6$ and $Cs_2AuInCl_6$.

Compound	a_0 (Å)	B_0 (GPa)	B'	V_0 (a.u.^{3})	E_0 (Ry)	E_{form}	t_G	μ
$Cs_2AgInCl_6$								
This work	10.60	31.01	5.31	2009.55	-59101.37	-1.609	0.94	0.44
Exp. work	10.470			3				
Other work	10.406							
	10.470							
$Cs_2AuInCl_6$								
This work	10.6356	31.7849	5.2955	2029.571	-86562.527312	-1.481	0.85	0.59
				7				
Similar compounds								
$Cs_2AuScCl_6$	10.53	34.38	6.03	19.89	-76324.63	-2.38	0.90	0.58
$Cs_2AuScBr_6$	11.08	23.20	5.52	2290	-102066.17	-2.00	0.89	0.53

The atomic electronic configurations used in this calculation are: Cs: $5s^2 5p^6 5d^0 6s^1 6p^0$, Ag: $4s^2 4p^6 4d^{10} 5s^1 5p^0$, Au: $5s^2 5p^6 5d^{10} 6s^1$, In: $4d^{10} 5s^2 5p^1$, Cl: $3s^2 3p^5$. Plane waves were utilized to expand the wave functions in the interstitial region [34]. To find the more stable phase between ferromagnetic (FM) and nonmagnetic (NM) states, research was carried out. Figures 2a) and 2b) show the energy optimization curves for Cs_2BInCl_6 compounds (B = Ag, Au). The analysis shows that the nonmagnetic (NM) state is more stable in terms of energy than the ferromagnetic (FM) phase.

3. Results and discussions

3.1. Structural properties

According to previous studies, the compounds Cs_2BInCl_6 under investigation were suggested to have a face-centered cubic (fcc) crystal structure with a space group of $Fm\bar{3}m$ (N°225) [4, 23, 35]. This structural assignment was based on the calculated values of the tolerance factor and octahedral ratio for these materials, which are provided in Table I.

The current work examines the formability of the double perovskite $A_2BB'X_6$ structure. The Goldschmidt tolerance factor (t_G) and the octahedral ratio (μ), also referred to as the radius ratio, are important parameters used in the engineering of halide perovskite materials. These parameters are key for predicting the stability and formability of perovskite compounds. The specific formulas used to calculate these factors are detailed in Refs. [4, 36].

$$t_G = \frac{r_A + r_X}{\sqrt{2}\left(\frac{r_B + r_{B'}}{2} + r_X\right)}, \quad (1)$$

$$\mu = \frac{r_B + r_{B'}}{2r_X}, \quad (2)$$

where r_A is the A cation radius, r_X is the X anion radius, r_B is the B metal radius, and $r_{B'}$ is the B′ metal radius, using the radii of Shannon [4].

It should be emphasized that the Goldschmidt tolerance and the octahedral factors for all the HDPs are placed in the stable ranges of $0.80 \leq t_G \leq 1.00$ and $0.41 \leq \mu \leq 0.9$, indicating certain formations of stable perovskite structures [4, 36]. The results, presented in Table I, show that the Cs_2BInCl_6 materials have stable perovskite structures.

The Shannon ionic radii were adopted as 1.88 Å for 12-coordinated Cs^+, 1.15 Å and 1.37 Å for 6-coordinated Ag^+ and Au^+, respectively, and 0.80 Å and 1.81 Å for 6-coordinated In^{3+} cations and Cl^- anions, respectively [14, 37].

The lattice parameters were initially taken as $a = 10.406$ Å for Cs_2BInCl_6, from earlier reported data [15, 38]. For better accuracy, these parameters were optimized using the energy optimization tool Available Wien2k which has resulted with modified value *i.e.* $a = 10.6005$ Å and $a = 10.6356$ Å for $Cs_2AgInCl_6$ and $Cs_2AuInCl_6$, respectively. In addition to determining the crystallographic stability, we calculated the formation energy, or E_{Form}, for Cs_2BInCl_6 to evaluate thermodynamic stabilities and gain understanding of the compounds' potential for synthesis that emerged from the application of the following formula [39]:

$$E_{\text{Form}} = \frac{E_{\text{Total}}^{Cs_2BInX_6} - (2E_{\text{Cs}} + E_B + E_{\text{In}} + 6E_X)}{10}, \quad (3)$$

where E_{tot} is the total energy of the unit cell, and $E(\text{Cs})$, $E(\text{B})$ (B = Ag, Au), $E(\text{In})$, and $E(\text{Cl})$ are the calculated total energies for the respective atoms in a cubic system. The findings from the computational assessment of formation energy are presented in Table I. Notably, these numerical outcomes exhibit negativity, indicating the favorable energetic nature of these phases from a thermodynamic perspective, thereby suggesting the feasibility of synthesizing these stable structures [40, 41].

TABLE II. Mechanical parameters of $Cs_2AgInCl_6$ and $Cs_2AuInCl_6$: elastic constants C_{11}, C_{12}, C_{44} (GPa), bulk modulus B (GPa), shear modulus G (GPa), Young's modulus E (GPa), Poisson's ratio ν, Pugh's ratio B/G, and anisotropy factor A.

	C_{11} (GPa)	C_{12} (GPa)	C_{44} (GPa)	B (GPa)	A	G	B/G	ν
$Cs_2AgInCl_6$	54.092	18.526	11.833	30.38	0.6654	13.9	2.18	0.60
$Cs_2AuInCl_6$	48.050	22.783	11.396	31.193	0.902	11.9	2.63	0.66
Similar compounds								
$Cs_2AgGaCl_6$	50.57	24.73	13.61	33.34	1.05	13.33	2.50	0.32
$Cs_2AgSbCl_6$	34.70	18.69	8.32	24.03	1.04	8.20	2.93	0.69

3.2. Elastic and mechanical properties

The examination of elasticity in crystals is crucial for understanding the complex correlation among a crystal's structure, its reaction to external pressure, and its mechanical characteristics. By delving deeply into this analysis, researchers and practitioners can discover novel opportunities for the progression of the field of materials science and engineering [42].

This investigation relies on the determination of 21 elastic constants (C_{ij}) [43], through the utilization of Density Functional Theory (DFT). In particular, in the case of cubic crystals, the stability conditions are simplified to three constants, namely C_{11}, C_{12}, and C_{44}, which can be verified through the introduction of the Born-Huang stability criteria [10, 44, 45]:

$$C_{11} + 2C_{12} > 0, \quad C_{11} - C_{12} > 0,$$
$$C_{11} > 0, \quad C_{44} > 0. \tag{4}$$

The criteria are met by the substances we studied, suggesting their theoretical mechanical stability. An in-depth analysis of the elastic properties of $Cs_2AgInCl_6$ and $Cs_2AuInCl_6$, as per the available data, unveils distinct mechanical characteristics that are vital for assessing their applicability in diverse engineering scenarios.

The elastic moduli values C_{11}, C_{12}, and C_{44} are identified as 54.092 GPa, 18.526 GPa, and 11.833 GPa, respectively, for $Cs_2AgInCl_6$, and 48.05 GPa, 22.783 GPa, and 11.396 GPa, respectively, for $Cs_2AuInCl_6$.

These results suggest that $Cs_2AgInCl_6$ exhibits greater stiffness in terms of C_{11}, enabling it to endure higher stress levels without distortion, indicating superior mechanical attributes compared to $Cs_2AuInCl_6$.

Conversely, the lower C_{12} value for $Cs_2AgInCl_6$ implies reduced capacity to withstand shear deformation under normal stress, hinting at inferior stability and performance under multi-axial loading conditions when compared to $Cs_2AuInCl_6$. Higher C_{12} values are typically associated with enhanced ductility and toughness. The similar C_{44} values for both materials signify equivalent shear modulus, with C_{44} values generally correlating with improved toughness and resistance to plastic deformation.

Other significant elastic constants are provided to comprehend the mechanical properties and behavior of crystalline materials: bulk modulus (B), shear modulus (G), Young's modulus (E), Poisson's ratio (ν), and Pugh's ratio (B/G) [14], which can be determined by employing the Voigt-Reuss-Hill equations Eq. (5) [18].

Assessing these elastic coefficients is essential for determining the solid material's ductility or brittleness, structural integrity, and anisotropy, among other properties. How materials respond to outside forces is seen by the elastic stiffness constants [44].

$$B = \frac{1}{2}(B_V + B_R), \quad A = \frac{2C_{44}}{C_{11} - C_{12}},$$
$$G = \frac{1}{2}(G_V + G_R), \quad \nu = \frac{3B - 2G}{6B + 2G},$$
$$G_V = \frac{1}{5}\big(C_{11} - C_{12} + 3C_{44}\big),$$
$$G_R = \frac{5C_{44}(C_{11} - C_{12})}{4C_{44} + 3(C_{11} - C_{12})},$$
$$B_V = B_R = \frac{1}{3}(C_{11} + 2C_{12}). \tag{5}$$

When the ratio B/G exceeds 1.75 or the value of ν surpasses 0.26, the nature of the material is identified as ductile; conversely, it exhibits brittleness [46]. Furthermore, when $A = 1$, the physical properties of perovskite materials are isotropic; otherwise, they are anisotropic [14, 46].

The results depicted in Table II demonstrate that the compounds being studied display characteristics that align with established standards, mirroring those of compounds such as $A_2AlAgCl_6$ (A = Rb, Cs), $Cs_2AgSbCl_6$, and $Cs_2AgGaCl_6$, as these materials also showcase conformity. This implication hints at the potential application of these perovskites in flexible or wearable optoelectronic devices.

The respective Pugh's ratio B/G values of 2.18 and 2.63 suggest the ductile characteristics of these compounds. Moreover, the analysis of Poisson's ratio can provide further evidence to substantiate the assertion mentioned above. Ductile materials typically have a Poisson's ratio threshold of $\nu > 0.26$ [18, 44], a criterion supported by prior research, which correlates well with the computed values of 0.60 and 0.66.

This suggests the potential application of such perovskites in flexible or wearable optoelectronic devices. Moreover, the physical characteristics of perovskite substances exhibit isotropy for $A = 1$ but display anisotropy

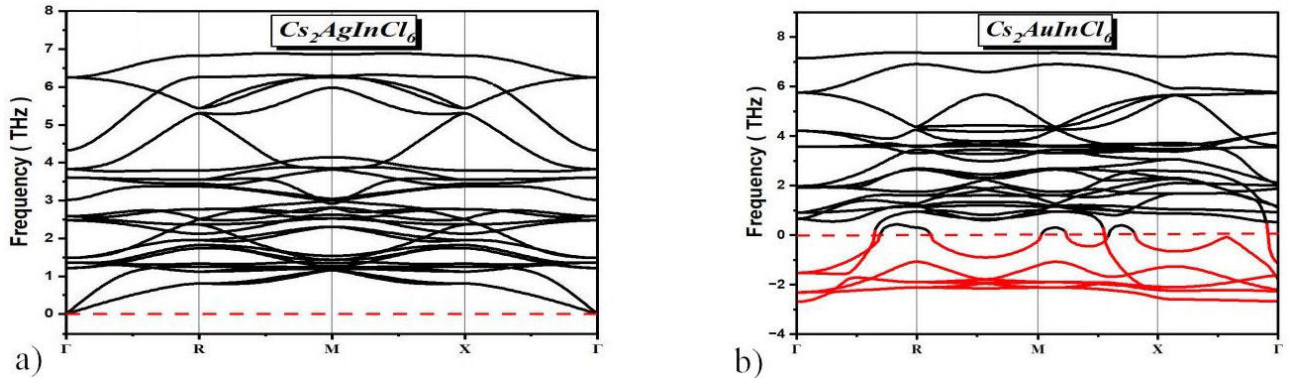

FIGURE 3. Phonon spectrum calculation for cubic double perovskite Cs_2BInCl_6: a) For $Cs_2AgInCl_6$, b) For $Cs_2AuInCl_6$.

otherwise [14]. The calculated values of 0.66 and 0.90, respectively, indicate that both chemicals exhibit anisotropic behavior. Other compounds that exhibit this behavior include $Cs_2AgSbCl_6$, $Cs_2AgGaCl_6$, and $A_2AlAgCl_6$ (A = Rb, Cs).quantities from 1 suggests that they differ, even though their numerical values are different. This suggests the potential application of such perovskites in flexible or wearable optoelectronic devices.

3.3. Phonon properties and dynamical stability

Our compounds, $Cs_2AgInCl_6$ and $Cs_2AuInCl_6$, were verified to be stable in both geometric and mechanical states under those conditions. We used the finite-displacement method to calculate their phonon dispersions in order to investigate the dynamical stability, employing the $2 \times 2 \times 2$ supercells [14]. The phonon spectra were calculated using the PHONOPY package in conjunction with the WIEN2K code, as shown in Fig. 3.

For these double perovskites, the cubic structure confirms phonon modes, as the primitive unit cell contains 10 atoms. Among these phonon modes, we identified the acoustic modes, characterized by approaching zero phonon frequency as going to the zone center Γ-point [23].

The soft phonon mode of $Cs_2AuInCl_6$ is prolonged up to approximately $-2.69\,\mathrm{cm}^{-1}$, as seen by the red line in Fig. 3b). Negative values in this region suggest a negative phonon spectrum and indicate that perovskites based on Au are probably unstable in the cubic phase. However, as evidenced by the positive phonon spectrum of the compound $Cs_2AgInCl_6$ illustrated in Fig. 3a), it exhibits stability in the cubic phase.

Nevertheless, the existence of imaginary phonon modes does not always imply that the structure is unstable, according to a recent study [47]. The investigation showed that the Au-based double perovskites had incredibly weak soft phonon modes in contrast to the Ag-based compounds. Given that perovskites with soft phonon modes can form cubic phases at high temperatures, we carried out further research on the characteristics of the cubic HDPs Cs_2BInCl_6.

3.4. Electronic properties

3.4.1. Band structures

Electron dispersion can be a highly useful way to distinguish between metals, semiconductors, insulators, and semimetals [36]. Moreover, the transitions between these states are critically important, as they fundamentally govern the system's behavior and functional properties [48].

When choosing a material to employ in energy-harvesting applications, determining its electronic energy band structure and total and partial densities of states (TDOS and PDOS) are crucial factors to consider [49]. The present work investigates the electronic properties of a series of compounds using first-principles computational methods.

Initially, the generalized gradient approximation (GGA-PBE functional) was employed. The results demonstrated a metallic character for $Cs_2AuInCl_6$, while $Cs_2AgInCl_6$ exhibited a band gap of 0.35 eV. However, these findings deviated significantly from the experimental data and previous theoretical studies.

Subsequently, the modified Becke–Johnson (mBJ) potential was utilized as an alternative approach. This method yielded band gap values of 3.24 eV and 2.05 eV for $Cs_2AgInCl_6$ and $Cs_2AuInCl_6$, respectively, leading to results that showed better agreement with the available experimental and theoretical data from prior investigations. This indicates that, due to its improved approximation of the exchange potential, the mBJ method corrects the underestimated band gap seen in GGA calculations by offering values that more accurately reflect the actual electronic structure.

It is found that these compounds share the same nature of band gap, namely a direct band gap. The band structure graphic shows that the conduction band minimum (CBM) and valence band maximum (VBM) overlap exactly at the first Brillouin zone's highest symmetry point, also known as the Γ-point. The arrangement indicates that Cs_2(Ag,Au)$InCl_6$ semiconductors have a noteworthy property: their estimated direct band gap can be precisely tuned.

Practically speaking, this means that the electron transitions are located ideally, which facilitates efficient electron excitation and enhances their potential for a wide range of

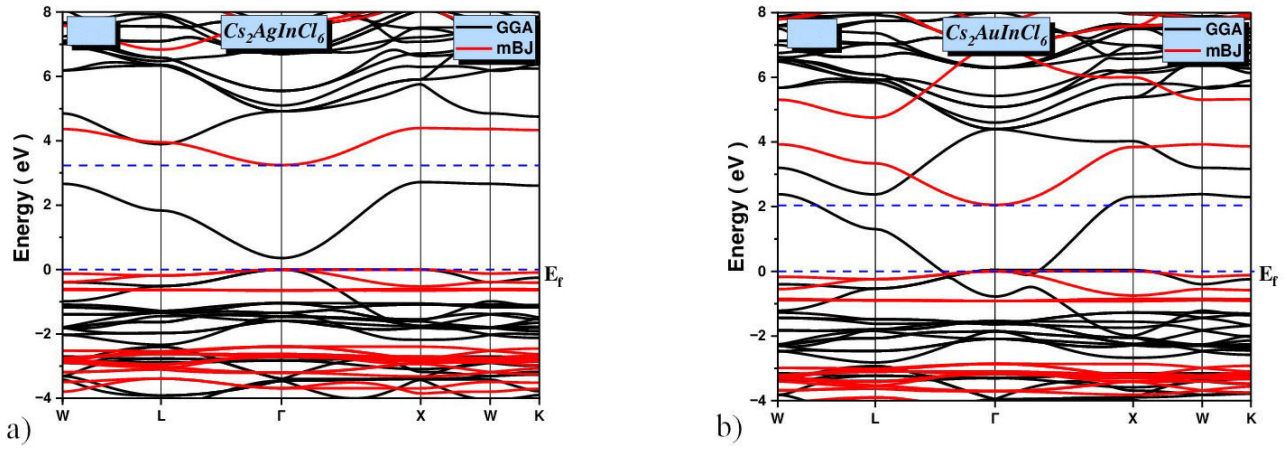

FIGURE 4. Electronic band structure for cubic double perovskite $Cs_2BInCl-6$, using both GGA and mBJ approaches: a) For $Cs_2AgInCl_6$, b) For $Cs_2AuInCl_6$.

TABLE III. The calculated band gap energy E_g (eV) of $Cs_2AgInCl_6$ and $Cs_2AuInCl_6$ using GGA and mBJ methods, compared with other theoretical and experimental works.

	GGA	mBJ	Other work	
	$\Gamma-\Gamma$	$\Gamma-\Gamma$	Theor	Exp
$Cs_2AgInCl_6$	0.355	3.245	3.33, 2.31, 3.01, 2.95	3.23, 3.53, 3.3, 3.24, 3.23
$Cs_2AuInCl_6$	0	2.052	/	/

optoelectronic applications. Without the lattice phonon contribution, these materials' intrinsic direct band gap feature permits light absorption through direct electronic transitions between valence band states and accessible conduction states.

Figures 4a) and 4b) illustrate the functional computation of the band structures for $Cs_2AgInCl_6$ and $Cs_2AuInCl_6$, respectively, along high-symmetry directions in k-space using both GGA and mBJ approaches. Table III summarizes the results of this investigation, which are in good agreement with many other theoretical and experimental conclusions obtained by different means.

The findings of this study emphasize the importance of carefully selecting suitable computational methodologies to accurately estimate material properties, as evidenced by the notable variations in the calculated band gaps. When analyzing the characteristics of novel functional materials, it is imperative to fully comprehend the advantages and disadvantages of various theoretical approaches. This highlights the necessity of carefully choosing the appropriate computational method to correctly depict the electronic configuration of complex materials.

3.4.2. Density of states

The electronic structures of Cs_2BInCl_6 compounds were examined by analyzing their total density of states (TDOS) and partial density of states (PDOS) spectra within the energy range of -5 to 5 eV, using both GGA-PBE and TB-mBJ approximations for comparison. The band gap was determined and confirmed utilizing the TDOS. In addition to identifying electron state contributions from different states within the band structure, as depicted in Figs 5a), 5b), 5c), and 5d), using PBE-GGA and TB-mBJ, the contribution of elements (Cs, Ag, Au, Cl) to the conduction band minimum (CBM) and valence band maximum (VBM) was highlighted.

This study of the density of states also provides additional information about the nature of chemical bonds. By analyzing the contributions of the different electronic orbitals, a deeper understanding of the interactions within the studied compounds is gained, which expands our knowledge of the mechanisms governing their behavior [50].

In Fig. 5c), it can be observed that for the compound $Cs_2AgInCl_6$, the valence band maximum (VBM) is primarily influenced by the presence of the Ag atom and halide atom (Cl). Conversely, Fig. 5d) demonstrates the dominance of the Au atom and halide atom (Cl) in the VBM for $Cs_2AuInCl_6$. Meanwhile, the conduction band minimum (CBM) is influenced collectively by the In atom and halide atoms (Cl) in both compounds.

To determine the specific orbital contributions to the VBM and CBM in the atoms, an analysis of the partial density of states (PDOS) was conducted. This analysis is illustrated in Figs. 6a), 6b), 6c), and 6d) for $Cs_2AgInCl_6$ and $Cs_2AuInCl_6$, using GGA and mBJ approaches. For the $Cs_2AgInCl_6$ compound shown in Figs. 6b) and 6d), the Ag-d orbital has a higher contribution in the valence band maximum (VBM) compared to the Ag-s and Ag-p orbitals, and shares this contribution with the Cl-p orbitals. Meanwhile, the In-s orbital shares with the Cl-p orbital in the conduction band minimum (CBM).

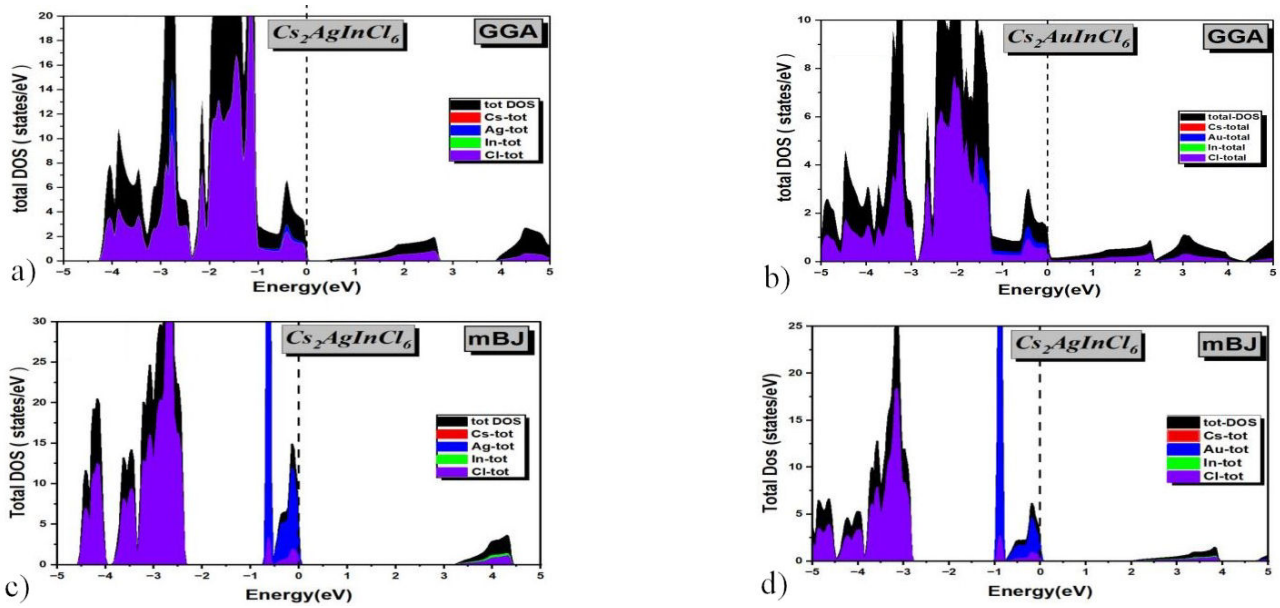

FIGURE 5. Total Density of State (TDOS) of Cs_2BInCl_6: a) For $Cs_2AgInCl_6$ using GGA, b) For $Cs_2AuInCl_6$ using GGA, c) For $Cs_2AgInCl_6$ using mBJ, d) For $Cs_2AuInCl_6$ using mBJ.

Similarly, for the $Cs_2AuInCl_6$ compound shown in Figs. 6b) and 6d), the Au-d orbitals have a higher contribution in the VBM and share this with the Cl-p orbitals, while the In-s orbital shares with the Cl-p orbital in the CBM.

3.5. Optical properties

Investigating a material's ability to harvest visible light energy can reveal its optical characteristics. This is usually accomplished by determining the band gap and absorption coefficients. Direct low band gap semiconductor materials are ideal because of their promising optoelectronic uses, such as solar cell photo-absorbers [51].

To understand the various ways that light interacts with our compounds, we have investigated their optical properties using the complex dielectric function:

$$\varepsilon(\omega) = \varepsilon_1(\omega) + i\varepsilon_2(\omega),$$

where ω denotes the photon frequency, and $\varepsilon_1(\omega)$ and $\varepsilon_2(\omega)$ are the real and imaginary parts of the dielectric function, respectively [52].

Materials with a high dielectric constant can store more electric charge at a given voltage, which makes them suitable for capacitors and insulators in high-voltage applications. The dielectric constant is thus a measure of a material's ability to store electrical energy in an electric field [53].

The imaginary part $\varepsilon_2(\omega)$ is obtained by summing the inter-band transitions from the occupied to unoccupied states, while the real part $\varepsilon_1(\omega)$ is recovered using the Kramers–Kronig relation [18, 54, 55].

In general, dielectric functions are directly related to the electronic structure of materials [56], describing how the material responds to electromagnetic radiation in terms of polarization. This function represents the linear response of the system to an external electromagnetic field [57].

From the real and imaginary parts of $\varepsilon(\omega)$, several other optical parameters can be derived, such as absorption coefficient $\alpha(\omega)$, refractive index $n(\omega)$, extinction coefficient $k(\omega)$, optical conductivity $\sigma(\omega)$, reflectivity $R(\omega)$, and energy loss function $L(\omega)$ [27, 58, 59].

In particular, the absorption coefficient and reflectivity are calculated as [60]:

$$\alpha(\omega) = \frac{2\pi\omega}{c}\sqrt{\frac{-\mathrm{Re}(\omega) + |\varepsilon|}{2}}, \tag{6}$$

$$R(\omega) = \frac{(n-1)^2 + k^2}{(n+1)^2 + k^2}. \tag{7}$$

According to our results, the static values of the real dielectric function $\varepsilon_1(0)$ for $Cs_2AuInCl_6$ and $Cs_2AuInCl_6$ are 2.42 and 1.83, respectively. As shown in Fig. 7a), $\varepsilon_1(\omega)$ decreases with increasing energy and crosses zero at 16.74 eV, corresponding to the screened plasma frequency. The smallest negative value occurs at 17.4 eV, implying that incident photons are strongly reflected, giving rise to a metallic character. This indicates potential applications of these compounds in UV radiation protection.

The optical transition mechanism is illustrated in Fig. 7b) by the imaginary part of the dielectric function $\varepsilon_2(\omega)$, which describes electronic transitions between The valence and conduction bands is represented by the threshold energy in the $\varepsilon_2(\omega)$ spectrum. In this instance, the threshold energies for $Cs_2AgInCl_6$ and $Cs_2AuInCl_6$ are found to be 3.2 eV and 2.16 eV, respectively, which is closer to the compounds' band gaps. The peak in the $\varepsilon_2(\omega)$ curve is produced by the internal transition of a single energy band, and its first maximum peak is called the *first absorption peak*. According to Fig. 7b), the

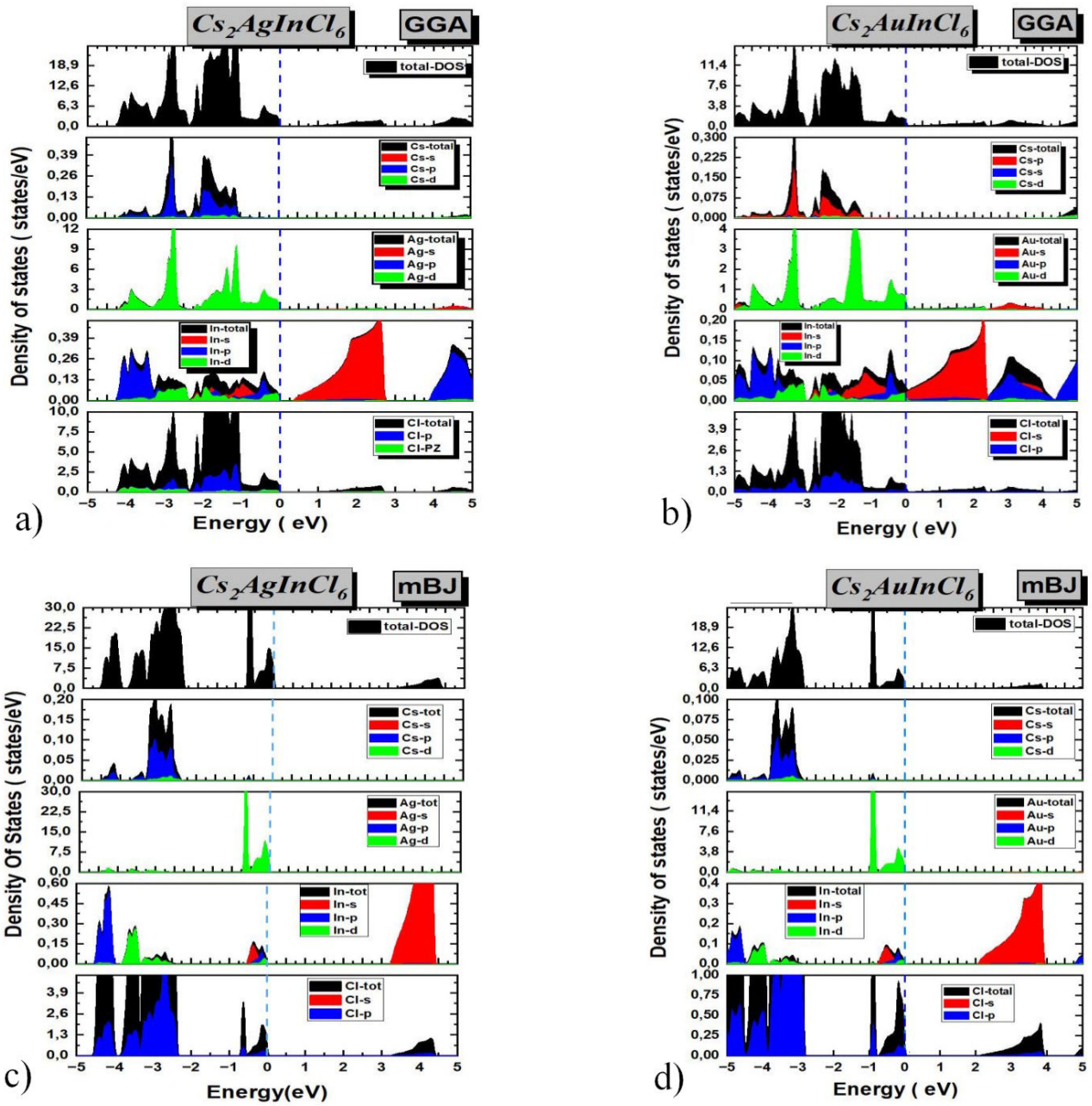

FIGURE 6. Partial Density of State (PDOS) of Cs_2BInCl_6: a) For $Cs_2AgInCl_6$ using GGA, b) For $Cs_2AuInCl_6$ using GGA, c) For $Cs_2AgInCl-6$ using mBJ, d) For $Cs-2AuInCl-6$ using mBJ

position of the first absorption peak of $\varepsilon_2(\omega)$ of $Cs_2AgInCl_6$ and $Cs_2AuInCl_6$ is about 4.28 eV and 3.66 eV, respectively. It may mainly be attributed to the transition of Cl-*p* electrons at VBM to hybrid orbitals of Cl-*p*, B (Ag, Au)-*s* and In-*s* at CBM. The real and imaginary sections of the dielectric function show peaks that occur in the ultraviolet (UV) and extreme ultraviolet (EUV) areas and have the potential to be used in optical filters at different frequency ranges. Among the two perovskites examined in this work, $Cs_2AgInCl_6$ exhibits superior dielectric characteristics over $Cs_2AuInCl_6$.

Another important factor determining the suitability of this material for solar cell applications lies in the absorption coefficient $\alpha(\omega)$. This parameter signifies the evaluation of the amount of light absorbed by a specific material. At approximately 3.3 eV (376 nm) for $Cs_2AgInCl_6$ and 2.05 eV (620 nm) for $Cs_2AuInCl_6$, direct optical transitions occur between the highest occupied states in the valence band and the lowest unoccupied levels in the conduction band (Fig. 7c). In the visible spectrum, both structures exhibit a low absorption coefficient and a high absorption coefficient in the UV and EUV spectra, making them a preferred choice for a range of

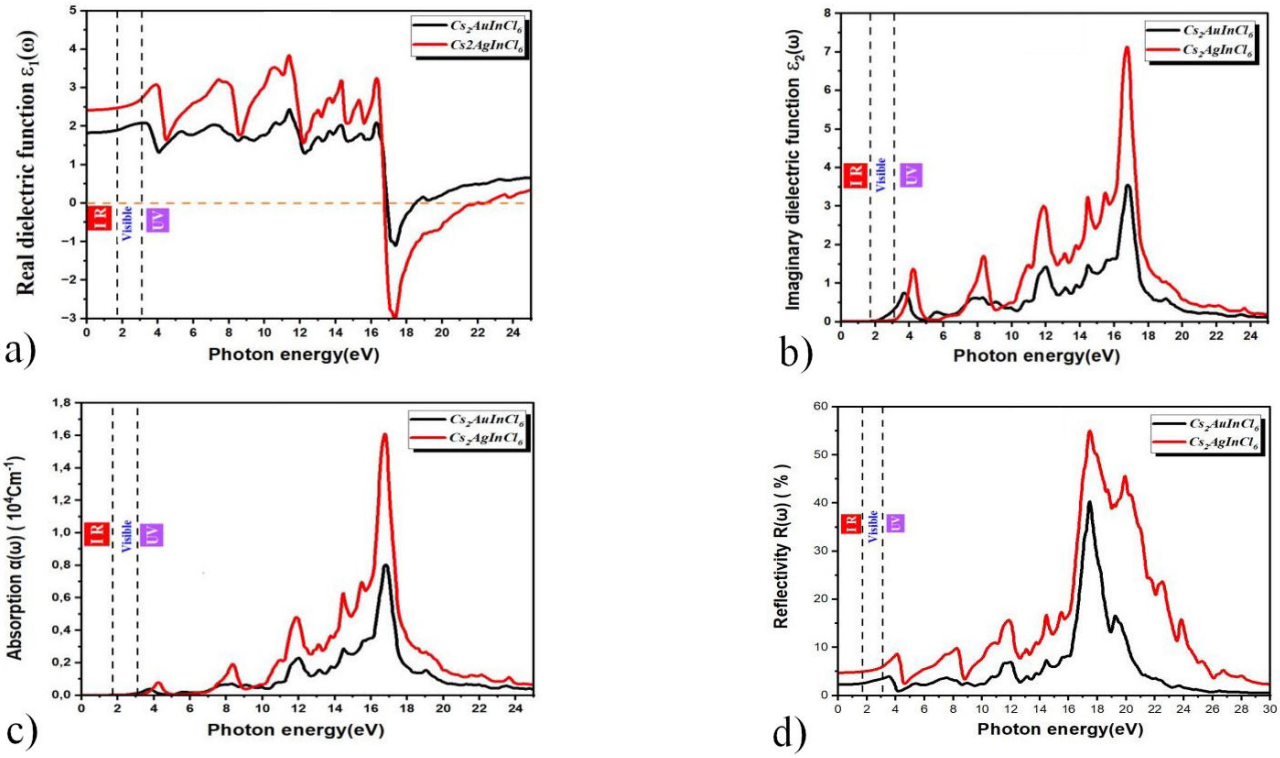

FIGURE 7. Optical parameters of Cs_2BInCl_6, using mBJ approximation: a) Real dielectric function. b) Imaginary dielectric function. c) Absorption. d) Reflectivity.

UV applications such as sunscreen, optical filters, and photography. The extreme ultraviolet EUV region exhibits the peak absorption, with values of 1.6×10^4 cm^{-1} and 0.8×10^4 cm^{-1} for $Cs_2AgInCl_6$ and $Cs_2AuInCl_6$, respectively, at 16.74 eV (74 nm).

For $Cs_2AgInCl_6$ and $Cs_2AuInCl_6$, the static reflectivity $R(0)$ values are 2.2% and 4.7%, respectively. In the 15–20 eV energy range, $Cs_2AgInCl_6$ exhibits a reflectivity peak of 55%; this is most noticeable at energies close to 17.5 eV (Fig. 7d). In the same energy range, $Cs_2AuInCl_6$ exhibits a reflectivity peak of 40%. The compound $Cs_2AgInCl_6$ demonstrates a significant resonance within the EUV energy spectrum, leading to a notable enhancement in the reflectivity of the material. Conversely, $Cs_2AuInCl_6$, a distinct compound, shows a less significant resonance within the same energy spectrum.

Overall, the thorough research offers extensive insights into the optical characteristics, electronic transitions, and possible uses of our compounds, including UV light used in medicine, phototherapy, semiconductor lithography, UV radiation protection, and optical filtering.

3.6. Thermoelectric properties

An analysis of the thermoelectric (TE) characteristics of a material involves evaluating its efficiency in converting heat energy into electrical energy and vice versa [61, 62]. The electronic conduction and thermoelectric phenomena exhibited by a material are intricately connected to its electronic band arrangement, with the primary influence stemming from factors such as the band gap magnitude, type of conductivity, concentration of charge carriers, and effective mass [63].

Thermoelectric materials have several significant applications, including energy harvesting and power generation. They are also used for cooling and temperature control, providing precise temperature control for electronic components such as CPUs, infrared detectors, and laser diodes. Additionally, they are employed in sensing and detection applications, including thermal imaging cameras and fire detection systems. Furthermore, wearable thermoelectric modules harness body heat to power mobile devices and sensors, enabling self-sustaining wearable technology [64, 65].

The thermoelectric transport parameters were calculated using the linearized Boltzmann transport equation (BTE), which is also solved by the BOLTZTRAP code [66, 67]. The BOLTZTRAP software interpolates the band structure obtained from DFT calculations and performs the necessary integrations (Fermi integrals) at different temperatures and Fermi levels.

ZT, or dimensionless figure of merit, is the parameter that controls thermoelectric material performance, which can be calculated using the following expression [68, 69]:

$$ZT = \frac{S^2\sigma}{\kappa}T, \tag{8}$$

where S is the Seebeck coefficient, σ is the electrical conductivity, $S^2\sigma$ is the power factor, T is the absolute temperature,

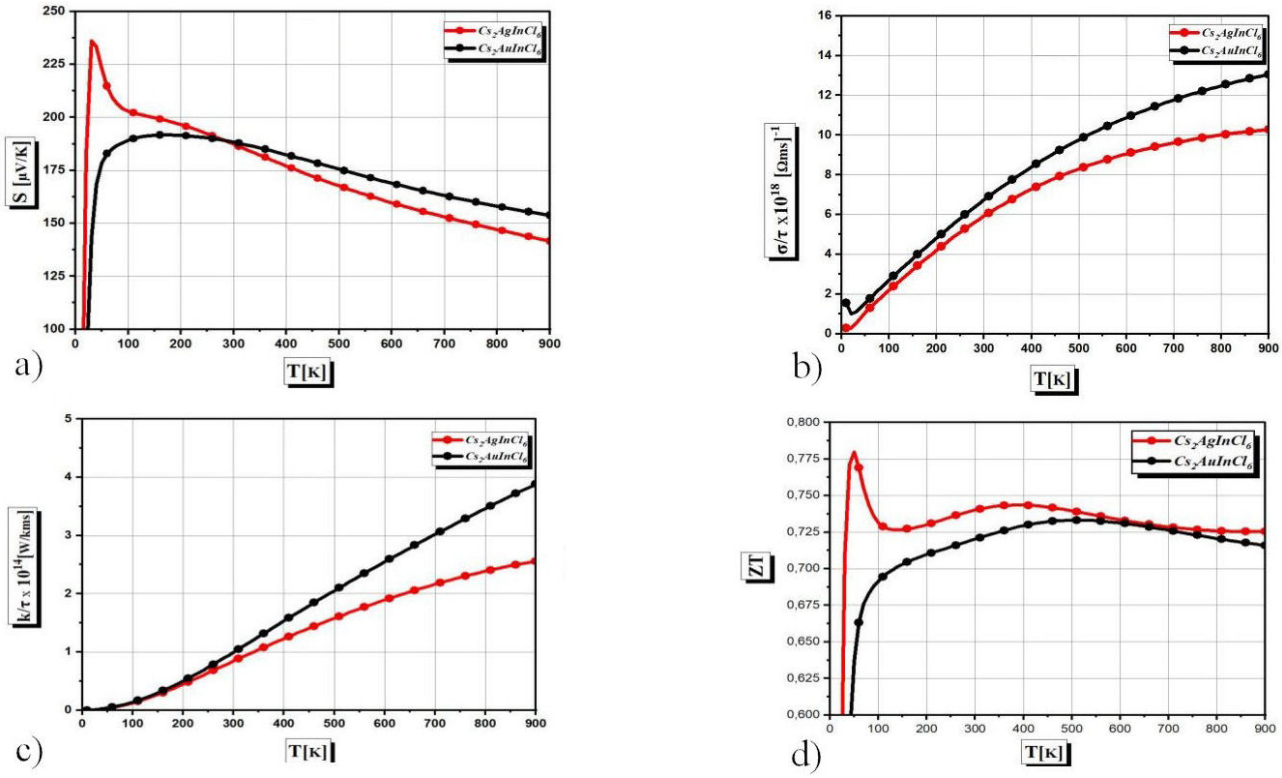

FIGURE 8. Thermoelectric parameters of Cs_2BInCl_6, using mBJ approximation: a) variation of Seebeck coefficient S as a function of temperature, b) variation of electrical conductivity, c) variation of thermal conductivity, d) variation of figure of merit ZT.

and κ is the total thermal conductivity, which is composed of an electronic part (κ_e) and a lattice part (κ_L). We do not consider the lattice part of the thermal conductivity here [30].

High-quality thermoelectric materials usually exhibit a confluence of several characteristics that improve their effectiveness. While lower thermal conductivity (κ) is an important factor for efficient thermoelectric materials, higher ZT values indicate improved thermoelectric efficiency. Other desirable properties include higher Seebeck coefficients (S) and higher electrical conductivity (σ) [70].

Figure 8a) depicts the variation in the Seebeck coefficients of Cs_2BInCl_6 compounds as temperature increases, indicating a decrease while still falling within the optimal range of 100–300 μV/K. At 300 K, the Seebeck coefficients were 188 μV/K for $Cs_2AuInCl_6$ and $Cs_2AgInCl_6$. Subsequently, at 900 K, the Seebeck coefficients dropped to 153 μV/K for $Cs_2AuInCl_6$, and 141 μV/K for $Cs_2AgInCl_6$. Despite the decline observed, these values continued to fall within the desired range for efficient thermoelectric performance.

The correlation between temperature and the estimated electrical conductivity (σ/τ) can be observed in Fig. 8b). It is apparent that the electrical conductivity (σ/τ) increases from 7×10^{18} $(\Omega \cdot \mathrm{m} \cdot \mathrm{s})^{-1}$ and 6×10^{18} $(\Omega \cdot \mathrm{m} \cdot \mathrm{s})^{-1}$ for $Cs_2AuInCl_6$ and $Cs_2AgInCl_6$, respectively, at 300 K, to 13×10^{18} $(\Omega \cdot \mathrm{m} \cdot \mathrm{s})^{-1}$ and 10×10^{18} $(\Omega \cdot \mathrm{m} \cdot \mathrm{s})^{-1}$ at 900 K for $Cs_2AuInCl_6$ and $Cs_2AgInCl_6$, respectively. The findings indicate that Au-based structures exhibit higher conductivity values compared to Ag-based structures.

Figure 8c) displays the variation in thermal conductivity (κ/τ), which increases from around 1×10^{14} (W/K·m·s) for both compounds at 300 K, then increases to 2×10^{14} and 2.5×10^{14} (W/K·m·s) for $Cs_2AgInCl_6$ and $Cs_2AuInCl_6$, respectively, at 600 K. It then further increases to 2.5×10^{14} and 3.8×10^{14} (W/K·m·s) for $Cs_2AgInCl_6$ and $Cs_2AuInCl_6$, respectively, at 900 K.

The crucial thermoelectric parameter, the figure of merit ZT, is presented in Fig. 8d). It has shown a small variation of 0.72 to 0.75 over the temperature range of 300–900 K.

Overall, the obtained results provide insightful information into the basic thermoelectric properties of the compound Cs_2BInCl_6, highlighting its potential as a thermoelectric material with significant power generation capabilities, particularly at low temperatures, and the ability to maintain reasonable thermoelectric efficiency over a broad temperature range. These results closely align with other relevant theoretical studies, such as those on CuX (X = Cl, Br) [71], particularly regarding the effect of temperature on thermoelectric properties. This offers the opportunity to be used in the industrial sector to convert thermal emissions from human bodies and other sources, such as engines in automobiles and ships, into energy. Reducing the use of fossil fuels and preventing global warming are two major benefits of such an application.

4. Conclusions

This study investigates the theoretical evaluation of the structural, stability, elastic, electronic, optical, and thermoelectric properties of the inorganic halide double perovskite compounds Cs_2BInCl_6 (B = Ag, Au) using GGA-PBE and TB-mBJ approximations. We find that both compounds maintain the typical cubic structure within the space group $Fm\overline{3}m$ (No. 225), as well as their optimal tolerance and octahedral parameters, in accordance with the crystallographic stability principle. The electronic examination reveals that the compounds exhibit a direct band gap. Furthermore, these substances demonstrate remarkable phase stability against degradation. These systems also exhibit mechanical stability, and their elastic characteristics suggest that they possess flexibility and ductility while displaying elastic anisotropy. The evaluation of the optical absorption coefficient indicates that the compounds display a low absorption coefficient, followed by multiple peaks across the UV and EUV spectra. The peaks observed in the graphs of the real and imaginary components of the dielectric function, in the visible, UV, and EUV regions, suggest a promising application in optical filters across various frequency ranges. Moreover, both compounds exhibit elevated electrical conductivity, low thermal conductivity, an increased Seebeck coefficient, and a higher figure of merit, positioning them as favorable candidates for thermoelectric applications.

1. A. Menedjhi, N. Bouarissa, S. Saib, and K. Bouamama, Halide double perovskite Cs2AgInBr6 for photovoltaic's applications: Optical properties and stability, *Optik*, **243** (2021) 167198.
2. S. Ghosh, H. Shankar, and Kar, Recent developments of lead-free halide double perovskites: a new superstar in the optoelectronic field, *Materials Advances*, **3** (2022) 3742-3765.
3. L. Muscarella and E. Hutter, Halide double-perovskite semiconductors beyond photovoltaics. *ACS Energy Lett* **7** (2022) 2128-2135.
4. Vishnoi, R. Seshadri, and A. K. Cheetham, Why are double perovskite iodides so rare?, *The Journal of Physical Chemistry C*, **125** (2021) 11756-11764.
5. C. Pareja-Rivera, D. Morett, D. Barreiro-ArgÃ$\frac{1}{4}$elles, Olalde-Velasco, and D. Solis- Ibarra, Lead-free halide perovskites, beyond solar cells and LEDs, *Journal of Physics: Energy*, **3** (2021) 032014.
6. M. R. Filip, X. Liu, A. Miglio, G. Hautier, and F. Giustino, Phase diagrams and stability of lead-free halide double perovskites Cs2BB' X6: B= Sb and Bi, B'= Cu, Ag, and Au, and X= Cl, Br, and I, *The Journal of Physical Chemistry C*, **122** (2018) 158-170.
7. S. Zerroug, F. A. Sahraoui, and N. Bouarissa, Elastic properties of AlxIn1- xPySb1- y and AlxGa1- xPySb1- y lattice matched to InAs substrate, *Materials Letters*, **60** (2006) 546-550.
8. G. Volonakis *et al*., Cs2InAgCl6: a new lead-free halide double perovskite with direct band gap, *The journal of physical chemistry letters*, **8** (2017) 772-778 .
9. J. Zhou, Z. Xia, M. S. Molokeev, X. Zhang, D. Peng, and Q. Liu, Composition design, optical gap and stability investigations of lead-free halide double perovskite Cs 2 AgInCl 6, *Journal of Materials Chemistry A*, **5** (2017) 15031-15037.
10. J. Luo *et al*., Cs2AgInCl6 double perovskite single crystals: parity forbidden transitions and their application for sensitive and fast UV photodetectors, *Acs Photonics*, **5** (2018) 398-405.
11. T. T. Tran, J. R. Panella, J. R. Chamorro, J. R. Morey, and T. M. McQueen, Designing indirect-direct bandgap transitions in double perovskites, *Materials Horizons*, **4** (2017) 688-693.
12. J. Luo *et al*., Efficient and stable emission of warm-white light from lead-free halide double perovskites, *Nature*, **563** (2018) 541-545.
13. N. Neelu, N. Pandey, and S. Chakrabarti, Synthesis, structural and optical properties of lead free Cs2CuBiCl6: A potential & promising eco-friendly double perovskite for solar cell applications, *Optical Materials*, **143** (2023) 114250.
14. C.-J. Yu, I.-C. Ri, H.-M. Ri, J.-H. Jang, Y.-S. Kim, and U.-G. Jong, First-principles study on structural, electronic and optical properties of halide double perovskite Cs 2 AgBX 6 (B= In, Sb; X= F, Cl, Br, I), *RSC advances*, **13** (2023) 16012-16022.
15. E. T. McClure, M. R. Ball, W. Windl, and M. Woodward, Cs2AgBiX6 (X= Br, Cl): new visible light absorbing, lead-free halide perovskite semiconductors, *Chemistry of Materials*, **28** (2016) 1348-1354.
16. A. Ullah, M. Khan, B. S. Almutairi, A. Laref, and A. Dahshan, Trans-polyacetylene doped Cs2AgBiBr6: Band gap reduction for high-efficiency lead-free double perovskite solar cells, *Results in Physics*, **60** (2024) 107654.
17. M. Kibbou, Z. Haman, N. Khossossi, I. Essaoudi, A. Ainane, and R. Ahuja, Computational insights into the superior efficiency of Cs2AgGa (Cl, Br) 6 double halide perovskite solar cells, *Materials Chemistry and Physics*, **294** (2023) 126978.
18. T.-Y. Tang, X.-H. Zhao, X.-N. Wei, D.-Y. Hu, L.-K. Gao, and Y.-L. Tang, Study on electronic, mechanical and optical properties of perovskite Cs2AgGaX6 (X= Cl, Br), *Journal of Nanoelectronics and Optoelectronics*, **16** (2021) 1521-1527.
19. S. Mahmud, M. Ali, M. Hossain, and M. Uddin, DFT aided prediction of phase stability, optoelectronic and thermoelectric properties of A2AuScX6 (A= Cs, Rb; X= Cl, Br, I) double perovskites for energy harvesting technology, *Vacuum*, **221** (2024) 112926.
20. T. Saha, M. M. H. Babu, M. Arifuzzaman, and J. Podder, Thermodynamic and dynamic stability in a new potential Cs 2 AgAsCl 6 perovskite: insight from DFT study, *Physical Chemistry Chemical Physics*, **24** (2022) 26609-26621.
21. M. Kibbou, Z. Haman, I. Essaoudi, and A. Ainane, Designing new halide double perovskite materials Rb2AgGaX6 (X: Br, Cl) with direct band gaps and high power conversion efficiency, *Journal of Solid State Chemistry*, **317** (2023) 123698.

22. A. Ayyaz *et al*., Comparative DFT-based investigation of physical properties of Cs2MBiBr6 (M= Ag, Cu, and Au) Perovskites: sustainable materials for renewable energy, *Computational Condensed Matter,* **38** (2024) e00885.

23. J. Breternitz *et al*., Mechanochemical synthesis of the lead-free double perovskite Cs2[AgIn]Br6 and its optical properties, Journal of Physics: Energy, **1** (2019) 025003.

24. Y. Liu, I. J. Cleveland, M. N. Tran, and E. S. Aydil, Stability of the halide double perovskite Cs2AgInBr6, *The Journal of Physical Chemistry Letters,* **14** (2023) 3000-3006.

25. N. Mathew, N. R. Kumar, and R. Radhakrishnan, First principle study of the structural and optoelectronic properties of direct bandgap double perovskite Cs2AgInCl6, *Materials today: proceedings,* **33** (2020) 1252-1256.

26. S. Shakeel, Song, H. A. Alsalmah, G. Murtaza, and T. Huang, Investigation of Pressure-Dependent Electronic and Optical Properties of Double Perovskites Cs 2 AgXY 6 (X= Bi, In; Y= Cl, Br), *Journal of Inorganic and Organometallic Polymers and Materials,* **34** (2024) 1040-1054.

27. R. Ranaivoson, A. Raoelina, H. Andrianiaina, and R. Hanitriarivo, Density Functional Theory and its applications in Nanotechnology, (2018).

28. Blaha, K. Schwarz, F. Tran, R. Laskowski, G. K. Madsen, and L. D. Marks, WIEN2k: An APW+ lo program for calculating the properties of solids, The *Journal of chemical physics,* **152** (2020).

29. T. Rauch, M. A. Marques, and S. Botti, Local modified Becke-Johnson exchangecorrelation potential for interfaces, surfaces, and two-dimensional materials, *Journal of chemical theory and computation,* **16** (2020) 2654-2660.

30. K. Bhamu *et al*., Improving the optical and thermoelectric properties of Cs 2 InAgCl 6 with heavy substitutional doping: a DFT insight, *RSC advances*, **11** (2021) 5521-5528.

31. A. Menedjhi, N. Bouarissa, and S. Saib, Strained Cs2AgInCl6 double perovskite material: band structure, optical spectra and mechanical stability, *Physica Scripta,* **97** (2022) 085801.

32. M. Houari *et al*., Structural, electronic and optical properties of cubic fluoroelpasolite Cs2NaYF6 by density functional theory, *Chinese Journal of Physics*, **56** (2018) 1756-1763.

33. S. Aldaghfag, A. Aziz, M. Ishfaq, M. Yaseen, and S. Jamshaid, First principles insights into Cs 2 XACl 6 (X= Sc, Y) compounds for energy harvesting applications, *Dig. J. Nanomater. Biostructures,* **19** (2024).

34. K. Zhang *et al*., Structural, electronic, optical, elastic, thermodynamic and thermal transport properties of Cs 2 AgInCl 6 and Cs 2 AgSbCl 6 double perovskite semiconductors using a first-principles study, *Physical Chemistry Chemical Physics*, **25** (2023) 31848-31868.

35. B. Bouadjemi, S. Bentata, A. Abbad, and W. Benstaali, Ab-initio study of optoelectronic and magnetic properties of the orthorhombic NdMnO3 perovskite, *Solid State Communications*, **207** (2015) 9-15.

36. E. Meyer, D. Mutukwa, N. Zingwe, and R. Taziwa, Lead-free halide double perovskites: a review of the structural, optical, and stability properties as well as their viability to replace lead halide perovskites, *Metals*, **8** (2018) 667.

37. R. D. Shannon, Revised effective ionic radii and systematic studies of interatomic distances in halides and chalcogenides, *Foundations of Crystallography,* **32** (1976) 751-767.

38. Z. Zhang *et al*., Potential applications of halide double perovskite Cs2AgInX6 (X= Cl, Br) in flexible optoelectronics: unusual effects of uniaxial strains, *The journal of physical chemistry letters,* **10** (2019) 1120-1125.

39. M. Houari *et al*., Electronic structure and thermoelectric properties of semiconductors K2GeSiX6 (X= F, Cl, Br and I) compounds: Ab-Initio investigation, in Spin, (2021), 11: World Scientific, 2150009.

40. M. Houari *et al*., Lead-free semiconductors with high absorption: insight into the optical properties of K2GeSnBr6 and K2GeSnI6 halide double perovskites, *JETP Letters*, **112** (2020) 364-369.

41. A. Ayyaz *et al*., DFT exploration of elastic, optoelectronic, and thermoelectric properties of stable and eco-friendly double perovskites Cs2YAuX6 (X= Cl, Br) for green energy applications, *Journal of Physics and Chemistry of Solids,* **188** (2024) 111936.

42. A. Zitouni *et al*., Insight into Structural, Electronic, Magnetic, and Elastic Properties of Full-Heusler Alloys Co 2 YPb (Y= Ti, V, Fe, and Mo): Ab Initio Study, *JETP Letters*, **112** (2020) 290-298.

43. B. Bouadjemi *et al*., Ab-initio investigation of optoelectronic properties for elpasolite Cs2NaVCl6 using GGA+ U approach: Band gap engineering, *Computational Condensed Matter,* **26** (2021) e00531.

44. T.-Y. Tang, X.-H. Zhao, D.-Y. Hu, Q.-Q. Liang, X.-N. Wei, and Y.-L. Tang, Theoretical exploration of mechanical, electronic structure and optical properties of aluminium based double halide perovskite, *RSC advances*, **12** (2022) 10209-10218.

45. F. Mouhat and F.-X. Coudert, Necessary and sufficient elastic stability conditions in various crystal systems, *Physical review B*, **90** (2014) 224104.

46. A. Sholagberu, W. Yahya, and A. Adewale, Pressure effects on the opto-electronic and mechanical properties of the double perovskite Cs2AgInCl6, *Physica Scripta,* **97** (2022) 085824.

47. J. Lahnsteiner and M. Bokdam, Anharmonic lattice dynamics in large thermodynamic ensembles with machine-learning force fields: Cs Pb Br 3, a phonon liquid with Cs rattlers, *Physical Review B*, **105** (2022) 024302.

48. N. Bouarissa, Electron valence charge densities in Hg1-xCdxTe mixed crystals, *Infrared physics & technology*, **39** (1998) 265-270.

49. S. Haid *et al*., Optical properties of half-metallic ferrimagnetic double perovskite Sr2CaOsO6 compound, *Solid State Communications*, **322** (2020) 114052.

50. S. Mnasri, S. A.-B. Nasrallah, N. Sfina, N. Bouarissa, and M. Said, Electronic, lattice vibration and mechanical properties of CdTe, ZnTe, MnTe, MgTe, HgTe and their ternary alloys, *Semiconductor science and technology*, **24** (2009) 095008.

51. M. A. Ali, R. A. Alshgari, A. A. Awadh Bahajjaj, and M. Sillanpää, The study of new double perovskites K2AgAsX6 (X= Cl, Br) for energy-based applications, *Journal of Taibah University for Science*, **17** (2023) 2170680.

52. A. Gueddim, S. Zerroug, and N. Bouarissa, Optical characteristics of ZnTe1- xOx alloys from first-principles calculations, *Journal of luminescence*, **135** (2013) 243-247.

53. T. Lantri *et al*., Ab initio exploration of A2AlAgCl6 (A= Rb, Cs): unveiling potentials for UV optoelectronic applications, *Journal of Molecular Modeling*, **30** (2024) 195.

54. S. Al-Qaisi *et al*., A comprehensive first-principles study on the physical properties of Sr2ScBiO6 for low-cost energy technologies, *Optical and Quantum Electronics*, **55** (2023) 1015.

55. E. Haque and M. A. Hossain, Electronic, phonon transport and thermoelectric properties of Cs2InAgCl6 from first-principles study, *Computational Condensed Matter*, **19** (2019) e00374.

56. B. K. Bareth, M. N. Tripathi, and R. Maravi, High photovoltaic performance of lead-free Cs2AgInCl6-xBrx perovskite solar cell using DFT and SCAPS-1D simulations, *Materials Today Communications*, **39** (2024) 108618.

57. B. K. Bareth and M. N. Tripathi, First-principles study of the effect of strain on the structural and optoelectronic properties of flexible photovoltaic material Cs2AgInBr6, *Modelling and Simulation in Materials Science and Engineering*, **32** (2024) 055004.

58. M. Houari *et al*., Optoelectronic properties of germanium iodide perovskites AGeI 3 (A= K, Rb and Cs): first principles investigations, *Optical and Quantum Electronics*, **51** (2019) 1-14.

59. N. Bouarissa, Energy gaps and refractive indices of AlxGa1-xAs, *Materials chemistry and physics*, **72** (2001) 387-394.

60. A. Soni, K. Bhamu, and J. Sahariya, Investigating effect of strain on electronic and optical properties of lead free double perovskite Cs2AgInCl6 solar cell compound: a first principle calculation, *Journal of Alloys and Compounds*, **817** (2020) 152758.

61. S. A. Mir and D. C. Gupta, Analysis of cage structured halide double perovskites Cs2NaMCl6 (M= Ti, V) by spin polarized calculations, *Journal of Alloys and Compounds*, **854** (2021) 156000 .

62. L. BENAHMEDI, A. BESBES, and R. DJELTI, First-Principles Investigation of Physical, Mechanical, Thermodynamics and Transport Properties of Tetragonal Double Perovskite Sr2MnSbO6: A DFT+ U+ SOC Study, *Materials Chemistry and Physics*, (2025) 130520 .

63. A. Boutramine *et al*., First-principles Investigations of Structural, Thermodynamic, Optoelectronic and Thermoelectric Properties of Rb2CuMF6 (M= As3+, Bi3+) Eco-friendly Halide Double Perovskites: Materials for Green Energy Applications, *Journal of Inorganic and Organometallic Polymers and Materials*, (2024) 1-18 .

64. S. D. Patil *et al*., Highly selective ppm level LPG sensors based on SnO2-ZnO nanocomposites operable at low temperature, *Sensors and Actuators B: Chemical*, **377** (2023) 133080.

65. I. Petsagkourakis, K. Tybrandt, X. Crispin, I. Ohkubo, N. Satoh, and T. Mori, Thermoelectric materials and applications for energy harvesting power generation, *Science and technology of advanced materials*, **19** (2018) 836-862 .

66. H. Bendjilali, S. Gheriballah, A. Chahed, H. Rozale, and M. N. Bousahla, Density functional theory investigations of structural, elastic, optoelectronic and thermoelectric properties of the lead-free niobium-based double perovskite oxides (Ba/Sr/Ca) 2GaNbO6: materials for optoelectronic devices, *Indian Journal of Physics*, **97** (2023) 4233-4245.

67. G. K. Madsen and D. J. Singh, BoltzTraA code for calculating band-structure dependent quantities, *Computer Physics Communications*, **175** (2006) 67-71.

68. M. Y. Sofi, M. S. Khan, and M. A. Khan, Control of spin on ferromagnetism and thermoelectric properties of K 2 GeMnX 6 (X= Cl, Br, I) halide perovskites: emerging candidates for semiconductor spintronics and thermoelectric applications, *Materials Advances*, **5** (2024) 4913-4931.

69. L. Benahmedi, A. Besbes, and R. Djelti, Structural, magnetic, elastic, and thermoelectric properties of Ba2InOsO6 double perovskite in the cubic phase: A DFT+ U study with spin-orbit-coupling, *Journal of Magnetism and Magnetic Materials*, **611** (2024) 172629.

70. M. H. Cherif *et al*., Investigating the multifaceted characteristics of Ba2FeWO6 double perovskite: insights from density functional theory, *Journal of Molecular Graphics and Modelling*, **132** (2024) 108834.

71. N. Bioud, K. Kassali, and N. Bouarissa, Thermodynamic properties of compressed CuX (X= Cl, Br) compounds: ab initio study, *Journal of Electronic Materials*, **46** (2017) 2521-2528.